ICCK Journal of Image Analysis and Processing
http://dx.doi.org/10.62762/JIAP.2026.481080

RESEARCH ARTICLE

Check for updates

RETRACTED: Adaptive Hyperspectral Direct Classification Method Based on Computational Spectral Imaging

Dingguo Wang[1,*] **and Yudi Chen**[1]

[1] School of Optoelectronic Engineering, Xi'an Technological University, Xi'an 710021, China

Abstract

Hyperspectral image classification is a central task in remote sensing information extraction. Conventional approaches follow a reconstruct-then-classify paradigm, which entails large data volumes, high computational cost, and poor real-time performance. This paper presents an adaptive hyperspectral direct classification method based on computational spectral imaging. A Digital Micromirror Device (DMD) is used to spectrally encode and modulate the incident light, enabling direct output of two-dimensional spatial classification results without reconstructing the three-dimensional spectral data cube. First, a classification-oriented encoding template is designed via Fisher discriminant analysis to maximize inter-class separability. Second, classification decisions are made in the measurement space using Bayesian posterior probabilities, where the class-conditional probability is modeled as a multivariate Gaussian distribution and the maximum a posteriori (MAP) criterion is adopted. Third, an adaptive encoding template optimization mechanism driven by posterior probability weighting is introduced, which progressively improves classification accuracy through iterative feedback. Experiments on the Indian Pines and Pavia University datasets demonstrate that the proposed method achieves overall accuracies of 66.97% and 72.96%, respectively, using only 15-dimensional measurements (8.4% and 14.6% of the original spectral dimensions), with several individual class accuracies exceeding those of the standard Support Vector Machine (SVM) method, thereby confirming the feasibility and generalizability of the classify without reconstruction paradigm.

Keywords: computational spectral imaging, hyperspectral classification, digital micromirror device, Fisher discriminant analysis, adaptive encoding template, posterior probability.

1 Introduction

Hyperspectral remote sensing captures spectral information across hundreds of contiguous narrow bands, producing a three-dimensional data cube with rich spatial-spectral features that supports fine-grained land-cover identification and unmixing

Submitted: 13 April 2026
Accepted: 01 May 2026
Published: 07 May 2026

Vol. 2, **No.** 2, 2026.
10.62762/JIAP.2026.481080

***Corresponding author:**
Dingguo Wang
wangdingguo@st.xatu.edu.cn

Citation
Wang, D., & Chen, Y. (2026). Adaptive Hyperspectral Direct Classification Method Based on Computational Spectral Imaging. *ICCK Journal of Image Analysis and Processing*, 2(2), 92–103.

analysis [1]. However, hyperspectral classification faces the "curse of dimensionality" and the "Hughes phenomenon" [2]. Conventional methods follow a "reconstruct-then-classify" paradigm [3]: the full spectral data cube is first acquired, and feature extraction and classification are then performed. This paradigm suffers from two inherent limitations: (1) large data acquisition volumes—obtaining the hyperspectral data cube requires scanning along the spatial or spectral dimension, leading to low temporal resolution [4]; and (2) high computational complexity—reconstruction and subsequent classification of the spectral data cube demand significant computational resources.

Computational spectral imaging provides a promising route to overcome these bottlenecks [5]. By introducing a spatial light modulator (DMD) into the optical front end, the incident light is encoded and modulated, and high-dimensional spectral information is compressed and projected into a low-dimensional measurement space [6]. Coded Aperture Snapshot Spectral Imaging (CASSI) [7] acquires compressed measurements in a single or a few exposures, after which reconstruction algorithms recover the spectral data cube. Nevertheless, CASSI reconstruction is computationally expensive and time-consuming [8–11]. For classification tasks, the goal is to obtain class labels rather than the complete spectral data; hence, reconstructing the data cube is unnecessary. Several studies have explored direct classification from compressed measurements [12–14], and recent work has demonstrated that target detection can be performed directly in the compressive measurement domain without reconstruction [15, 16], yet existing methods typically employ fixed encoding templates not optimized for classification and lack adaptive adjustment mechanisms.

Recent advances in deep learning have substantially improved hyperspectral classification performance. Convolutional neural networks (CNNs) [17], transformer-based architectures [18], and graph neural networks [19] have demonstrated superior accuracy by capturing spatial-spectral features in an end-to-end manner. More recently, attention-based hybrid networks [20–24] have further advanced classification accuracy by integrating multi-scale feature extraction with adaptive attention mechanisms. However, these methods operate on the complete spectral data cube and are not applicable to compressed measurements. In the domain of computational spectral imaging, adaptive coded aperture design has attracted increasing attention [25, 26], and end-to-end optimization frameworks have been proposed to jointly learn the encoding and reconstruction [27, 28]. Nevertheless, these works focus on reconstruction quality rather than classification performance. Probabilistic classification methods, including Gaussian mixture models [29], naive Bayes classifiers [30], and variational inference approaches [38], offer a principled framework for uncertainty quantification and have been widely adopted in hyperspectral analysis. However, their application to direct classification from compressed measurements remains largely unexplored.

To address these issues, an adaptive hyperspectral direct classification method based on computational spectral imaging is proposed. The main contributions are: (1) A "classify without reconstruction" framework is introduced, where classification is performed directly in the measurement space through DMD encoding, bypassing spectral data cube reconstruction; (2) An encoding template is designed via Fisher discriminant analysis to maximize inter-class separability, orienting the template toward classification rather than reconstruction; (3) An adaptive encoding template optimization mechanism driven by posterior probability weighting is proposed, which iteratively adjusts both the encoding template and prior probabilities to improve classification accuracy; (4) An X-matrix extension method is proposed to handle spectral aliasing caused by two-dimensional spatial dispersion, enabling encoding template design for the 2D spatial domain; (5) The method is validated on two benchmark datasets—Indian Pines and Pavia University—demonstrating its generalizability across datasets with different spatial resolutions and spectral characteristics.

2 Related Work

Computational spectral imaging. Computational spectral imaging incorporates encoding and modulation elements into the optical system, compressing the three-dimensional spectral data cube into a two-dimensional measurement image [32]. The CASSI system [7] uses a coded aperture and a dispersive prism for joint spectral-spatial encoding. Kittle et al. [34] proposed a multi-frame CASSI system to improve reconstruction quality. DMD-based spectral encoding systems have drawn considerable attention due to their flexible programmable control [33, 35], providing a hardware basis for adaptive spectral imaging. Recent work has explored deep learning-based reconstruction for CASSI [8, 9, 36], achieving significant improvements in reconstruction quality. End-to-end coded aperture design frameworks have also been proposed [27], which jointly optimize the encoding and downstream tasks. Adaptive coded aperture design methods [25, 39] have also been proposed to optimize the sensing matrix for specific tasks.

Hyperspectral classification. Among conventional methods, SVM [2] is widely used for its strong generalization under small-sample conditions; spectral-spatial joint classification methods [31, 40] improve accuracy by incorporating spatial neighborhood information. For deep learning, Chen et al. [17] proposed a CNN-based classification framework, Hong et al. [41] introduced a multimodal deep learning approach, and Hong et al. [18] developed SpectralFormer for spectral-spatial feature extraction. More recently, attention-based and transformer architectures [20–22, 24, 37, 42] have further advanced classification accuracy. All these methods operate on the complete spectral data cube and cannot be directly applied to compressed measurements.

Direct classification from compressed measurements. Bacca et al. [14] proposed a coupled deep learning framework for jointly designing the coded aperture and the classifier for compressive image classification; Zhang et al. [13] proposed a 3D coded convolutional neural network for direct classification from compressive measurements. More recently, Yang et al. [15] established a restricted distribution property theory that preserves discriminative information without reconstruction, and further proposed a Triplet Transformer for compressive hyperspectral target detection [16]. These methods demonstrate the feasibility of direct classification or detection from compressed measurements; however, they all use fixed encoding templates without considering the effect of the template on classification performance, and lack adaptive adjustment mechanisms.

Probabilistic classification methods. Probabilistic approaches provide a principled framework for classification under uncertainty. In hyperspectral analysis, Gaussian mixture models and Bayesian classifiers have been widely adopted [29, 30]. Variational inference methods [38] and expectation-maximization algorithms have been employed for parameter estimation. The proposed method adopts a Bayesian posterior probability framework for classification in the measurement space, which naturally integrates with the adaptive encoding template optimization through posterior probability weighting.

3 Method

3.1 System Architecture

The system architecture is shown in Figure 1, consisting of an optical front end and an algorithmic back end. The optical front end comprises a dispersive system, a DMD encoding modulation module, and a beam-combining system, which encode and modulate the incident light into low-dimensional measurements. The algorithmic back end consists of a classification decision module and an adaptive optimization module, which perform classification in the measurement space and adjust the encoding template based on classification results, respectively. The workflow proceeds as follows: the incident light is dispersed, spectrally modulated by the DMD according to the encoding template, and converged by the beam-combining system onto the detector; the classification module makes decisions in the measurement space based on Bayesian posterior probability; if the classification accuracy falls below a predefined target (set to 0.80 in this study as a convergence criterion for the iterative process), the encoding template is adjusted via posterior probability weighting, and the next iteration begins. It should be noted that this target accuracy serves solely as a stopping criterion for the iterative optimization and does not represent the expected or achievable accuracy of the method.

3.2 Reference Spectral Library Construction

Let the hyperspectral data be $\mathbf{X} \in \mathbb{R}^{H\times W\times P}$, where H and W are the spatial dimensions and P is the number of spectral bands. A reference spectral library $\mathcal{S} = \{\mathbf{s}_c\}_{c=1}^{N}$ is constructed from training samples, where $\mathbf{s}_c$ is the set of spectral vectors for class c and N is the total number of classes. The class-wise statistics are computed as:

$$\boldsymbol{\mu}_c = \frac{1}{n_c}\sum_{\mathbf{s}\in\mathcal{S}_c}\mathbf{s},\ \boldsymbol{\Sigma}_c = \frac{1}{n_c-1}\sum_{\mathbf{s}\in\mathcal{S}_c}(\mathbf{s}-\boldsymbol{\mu}_c)(\mathbf{s}-\boldsymbol{\mu}_c)^\top \quad (1)$$

where $\boldsymbol{\mu}_c \in \mathbb{R}^P$ is the mean spectral vector of class c, $\boldsymbol{\Sigma}_c \in \mathbb{R}^{P\times P}$ is the within-class covariance matrix, and n_c is the number of training samples for that class. The prior probability is defined as $P(c) = n_c/\sum_{j=1}^{N} n_j$.

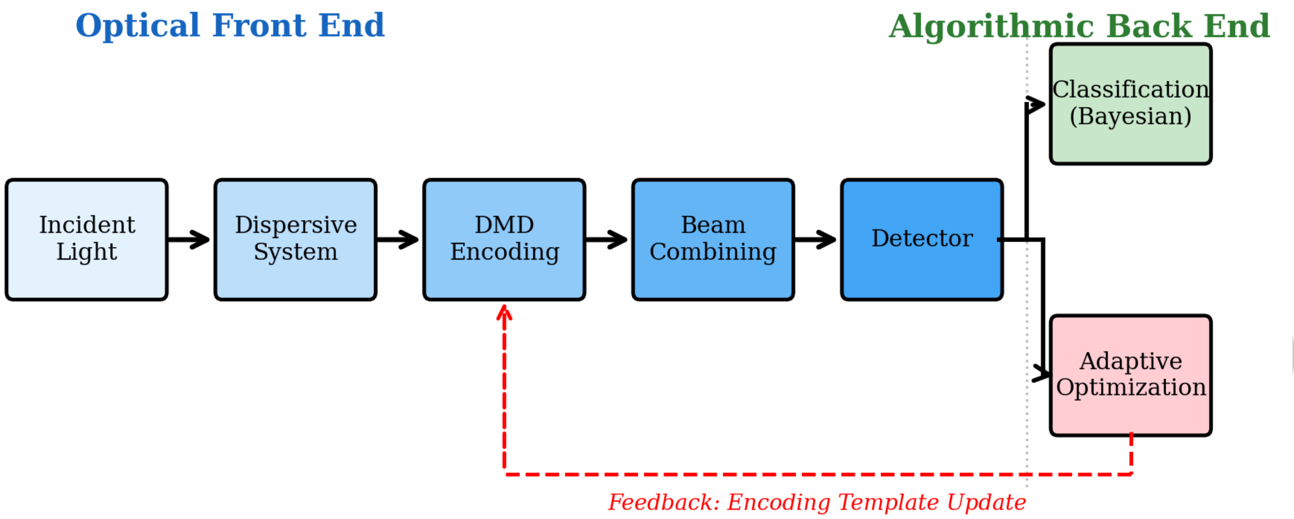

Figure 1. Workflow of the adaptive hyperspectral direct classification system.

3.3 Fisher Discriminant-Based Encoding Template Design

Conventional CASSI encoding templates are designed for reconstruction [7]; in contrast, the proposed template is designed to maximize inter-class separability. The X-matrix is defined as:

$$\mathbf{X}_{\text{mat}} = [\boldsymbol{\mu}_1 - \bar{\mathbf{s}}, \ldots, \boldsymbol{\mu}_N - \bar{\mathbf{s}}] \in \mathbb{R}^{P \times N} \tag{2}$$

where $\bar{\mathbf{s}} = \frac{1}{N}\sum_{c=1}^{N} \boldsymbol{\mu}_c$ is the global mean of all class centroids. Fisher discriminant analysis maximizes the criterion:

$$J(\mathbf{W}) = \frac{|\mathbf{W}^\top \mathbf{S}_B \mathbf{W}|}{|\mathbf{W}^\top \mathbf{S}_W \mathbf{W}|} \tag{3}$$

where the between-class scatter matrix is $\mathbf{S}_B = \sum_{c=1}^{N} n_c(\boldsymbol{\mu}_c - \bar{\mathbf{s}})(\boldsymbol{\mu}_c - \bar{\mathbf{s}})^\top \in \mathbb{R}^{P \times P}$ and the within-class scatter matrix is $\mathbf{S}_W = \sum_{c=1}^{N} n_c \boldsymbol{\Sigma}_c \in \mathbb{R}^{P \times P}$. The generalized eigenvalue problem $\mathbf{S}_B \mathbf{w} = \lambda \mathbf{S}_W \mathbf{w}$ is solved, and the eigenvectors $\mathbf{w}_1, \mathbf{w}_2, \ldots, \mathbf{w}_K$ corresponding to the K largest eigenvalues $\lambda_1 \geq \lambda_2 \geq \cdots \geq \lambda_K$ are selected to form the encoding template $\mathbf{W} = [\mathbf{w}_1, \mathbf{w}_2, \ldots, \mathbf{w}_K] \in \mathbb{R}^{P \times K}$. Figure 2 shows the coefficient distribution of the Fisher discriminant encoding template.

3.4 Spectral Modulation and Measurement Acquisition

The DMD encodes and modulates the incident spectrum $\mathbf{s} \in \mathbb{R}^P$ to produce K-dimensional measurements:

$$\mathbf{m} = \mathbf{W}^\top \mathbf{s} + \boldsymbol{\epsilon} \tag{4}$$

where $\mathbf{m} \in \mathbb{R}^K$ is the measurement vector and $\boldsymbol{\epsilon} \in \mathbb{R}^K$ represents additive measurement noise. Since DMD control signals are restricted to non-negative digital values, a time-division scheme is adopted: the first exposure uses $\mathbf{W}^+ = \max(\mathbf{W}, 0)$ to obtain $\mathbf{m}^+$, and the second uses $\mathbf{W}^- = \max(-\mathbf{W}, 0)$ to obtain $\mathbf{m}^-$, yielding the final measurement $\mathbf{m} = \mathbf{m}^+ - \mathbf{m}^-$.

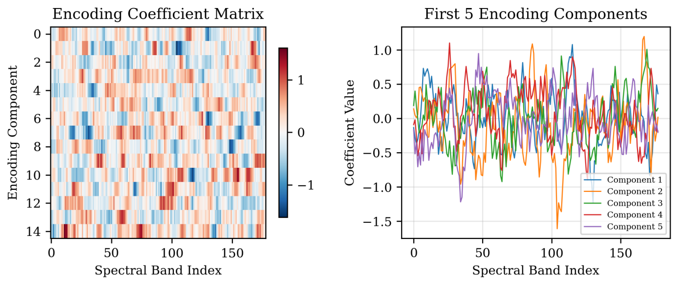

Figure 2. Visualization of the Fisher discriminant encoding template: (a) encoding coefficient matrix; (b) first 5 encoding components.

For 2D spatial scenes, spectral aliasing occurs after dispersion (see Figure 3), where adjacent row pixels are spectrally shifted by one band. The X-matrix is extended to the $\mathbf{X}'$-matrix:

$$\mathbf{X}'[i : i+P,\ iN : (i+1)N] = \mathbf{X}_{\text{mat}},\ i = 0, 1, \ldots, M-1 \tag{5}$$

where M denotes the number of spatial rows. Eigenvalue decomposition of $\mathbf{R}' = \mathbf{X}'(\mathbf{X}')^\top$ is then performed to obtain the encoding template for the 2D spatial domain.

3.5 Posterior Probability-Based Classification

The posterior probability is computed via Bayes' theorem:

$$P(c \mid \mathbf{m}) = \frac{P(c) \cdot P(\mathbf{m} \mid c)}{\sum_{j=1}^{N} P(j) \cdot P(\mathbf{m} \mid j)} \tag{6}$$

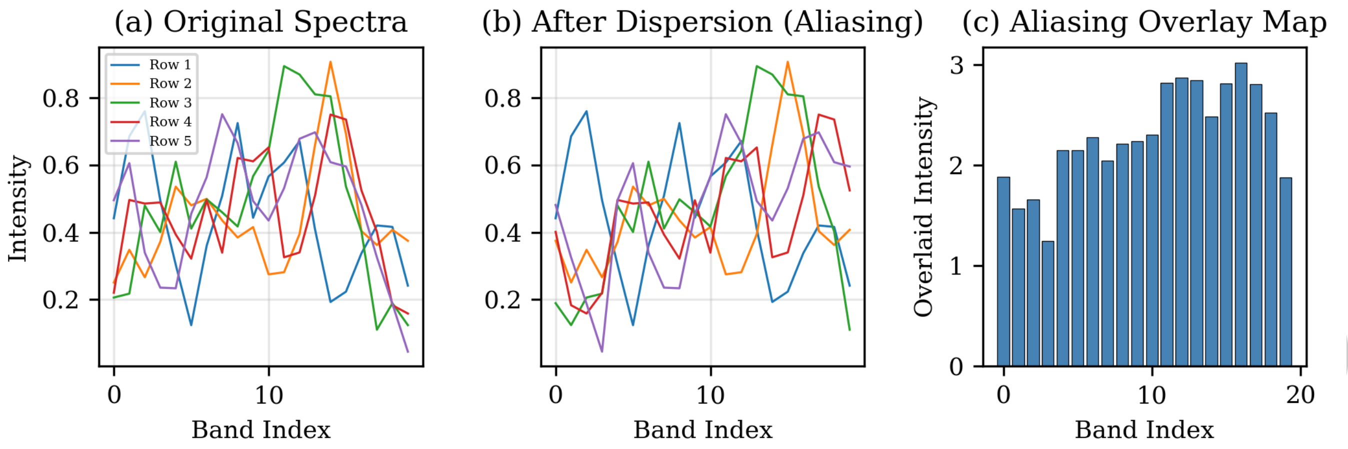

Figure 3. Spectral aliasing in the 2D spatial domain: (a) original spectra; (b) aliasing after dispersion; (c) aliasing overlay map.

where $P(c)$ is the prior probability of class c and $P(\mathbf{m} \mid c)$ is the class-conditional probability (likelihood). The class-conditional probability is modeled by a multivariate Gaussian distribution:

$$P(\mathbf{m} \mid c) = \frac{1}{(2\pi)^{K/2}|\boldsymbol{\Sigma}_c^m|^{1/2}} \times \exp\left(-\frac{1}{2}(\mathbf{m} - \boldsymbol{\mu}_c^m)^\top (\boldsymbol{\Sigma}_c^m)^{-1}(\mathbf{m} - \boldsymbol{\mu}_c^m)\right) \tag{7}$$

with $\boldsymbol{\mu}_c^m = \mathbf{W}^\top \boldsymbol{\mu}_c \in \mathbb{R}^K$ and $\boldsymbol{\Sigma}_c^m = \mathbf{W}^\top \boldsymbol{\Sigma}_c \mathbf{W} \in \mathbb{R}^{K \times K}$ as the mean vector and covariance matrix in the measurement space, respectively. The classification result is the class with the maximum posterior probability: $\hat{c} = \arg\max_c P(c \mid \mathbf{m})$, which corresponds to the MAP decision rule. To ensure positive definiteness of the covariance matrix, shrinkage regularization is applied:

$$\boldsymbol{\Sigma}_c^{\text{reg}} = (1-\alpha)\boldsymbol{\Sigma}_c^m + \alpha \cdot \frac{\text{tr}(\boldsymbol{\Sigma}_c^m)}{K}\mathbf{I}_K \tag{8}$$

where $\alpha \in (0, 1)$ is the shrinkage parameter and $\mathbf{I}_K \in \mathbb{R}^{K \times K}$ is the identity matrix.

3.6 Adaptive Encoding Template Optimization

The adaptive optimization consists of two core strategies. **Prior probability update:** Prior probabilities are updated based on the posterior probabilities of high-confidence pixels (maximum posterior probability > 0.7):

$$P_{\text{new}}(c) = (1-\eta)P_{\text{old}}(c) + \eta\hat{P}(c) \tag{9}$$

where $\hat{P}(c)$ is the average posterior probability of high-confidence pixels for class c and $\eta \in (0, 1)$ is the learning rate that controls the update step size. **Encoding template adjustment:** The confusion-weighted Fisher discriminant direction is computed from posterior probability weighting and conservatively fused with the current template:

$$\mathbf{W}_{\text{new}} = (1-\beta)\mathbf{W}_{\text{old}} + \beta\mathbf{W}_{\text{Fisher}}^{\text{weighted}} \tag{10}$$

where $\beta \in (0, 1)$ is the fusion learning rate and $\mathbf{W}_{\text{Fisher}}^{\text{weighted}}$ is the encoding template obtained from the confusion-weighted Fisher discriminant analysis. This weighting strategy gives classes with larger posterior probabilities greater influence on the encoding coefficients, thereby amplifying the posterior probability differences among classes.

4 Experiments

4.1 Datasets and Experimental Setup

Experiments were conducted on two widely used hyperspectral datasets to evaluate both the effectiveness and generalizability of the proposed method.

Indian Pines. This dataset was acquired by the AVIRIS sensor with a spatial size of 145×145 [2]. The original 220 spectral bands were reduced to 178 effective bands after removing water absorption and other noisy bands. The dataset contains 16 land-cover classes (including alfalfa, corn, grass, soybean, wheat, and woods).

Pavia University. This dataset was acquired by the ROSIS sensor over Pavia, northern Italy, with a spatial size of 610×340 and 103 spectral bands. The dataset contains 9 land-cover classes (including asphalt, meadows, gravel, trees, and bare soil). This dataset features higher spatial resolution (1.3 m) and fewer spectral bands compared with Indian

Pines, thereby providing a complementary test of the method's generalizability.

For each dataset, 10% of the samples were randomly selected for training, with the remainder used for testing. The parameters were set as follows: encoding dimension $K = 15$, maximum iterations 10, convergence threshold 0.80 (used solely as a stopping criterion for the iterative process), learning rate η linearly increasing from 0.1 to 0.3, fusion learning rate $\beta = 0.3$, shrinkage parameter $\alpha = 0.1$, and spatial smoothing window 5×5. The compared methods include: (1) SVM: RBF-kernel SVM in the original spectral space; (2) PCA (30-dim) + SVM: PCA dimensionality reduction followed by SVM; (3) Fisher encoding + SVM: SVM in the measurement space after Fisher discriminant encoding; (4) Non-adaptive spectral modulation: initial Fisher encoding template without iterative optimization.

4.2 Experimental Results on Indian Pines

4.2.1 Classification Accuracy Comparison

Table 1 and Figure 4 compare the classification accuracy of all methods on the Indian Pines dataset. SVM achieves the highest overall accuracy (OA) of 78.28%, which is expected since it operates on the full 178-dimensional spectral space. The proposed adaptive spectral modulation method attains an OA of 66.97%; although lower than SVM, it uses only 15-dimensional measurements—8.4% of the original spectral data—achieving an approximately 11.9-fold data compression.

Table 1. Classification accuracy comparison on Indian Pines.

Method	OA	AA	Kappa
SVM	**0.7828**	**0.6646**	**0.7497**
PCA+SVM	0.7539	0.6199	0.7158
Fisher+SVM	0.7511	0.6109	0.7121
Non-adaptive mod.	0.6435	0.5658	0.5918
Adaptive mod.	0.6697	0.5846	0.6216

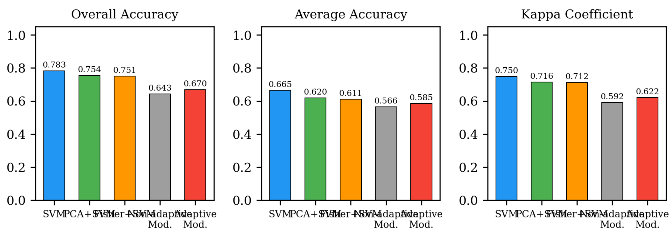

Figure 4. Classification performance comparison on Indian Pines.

Notably, the proposed method outperforms SVM on several classes (Table 2), such as Soybean-notill (97.94% vs. 68.80%), Grass-trees (98.63% vs. 97.26%), Stone-Steel-Towers (95.24% vs. 86.90%), and Bldg-Grass-Tree-Drives (50.57% vs. 45.69%). This indicates that the Fisher discriminant encoding template effectively captures discriminative spectral features of these classes, yielding better inter-class separation in the low-dimensional measurement space. For Soybean-notill in particular, the accuracy substantially exceeds that of SVM, suggesting that the discriminative information of this class is concentrated along the directions captured by the Fisher encoding. However, for classes with few samples, such as Corn and Alfalfa, the proposed method shows noticeably lower accuracy than SVM, indicating that low-dimensional encoding struggles to learn the class distribution when training samples are scarce.

4.2.2 Adaptive Iterative Optimization Analysis

Figure 5 shows the classification accuracy variation during adaptive iteration. At the first iteration (initial Fisher encoding template), the OA is 64.35%; after the prior probability update, the OA at the second iteration drops slightly to 63.80%, and subsequently converges to approximately 61.88%. Both AA and the Kappa coefficient show a similar declining trend. The accuracy decline during iteration is attributed to the fact that the current adaptive strategy updates only the prior probabilities while keeping the Fisher encoding template fixed; adjusting the priors may cause certain class priors to deviate from the true distribution, degrading classification performance. This phenomenon indicates that updating priors alone is insufficient to compensate for the limitations of the encoding template; simultaneous adjustment of the encoding template is required for sustained accuracy improvement. After spatial smoothing post-processing, the final OA increases to 66.97%, a 2.62 percentage point improvement over the non-adaptive method (64.35%), confirming the effectiveness of spatial smoothing. Spatial smoothing exploits the spatial autocorrelation in hyperspectral imagery, correcting low-confidence pixels via neighborhood majority voting and effectively reducing "salt-and-pepper noise" in the classification results.

4.3 Experimental Results on Pavia University

To evaluate the generalizability of the proposed method, experiments were also conducted on the Pavia University dataset, which differs from Indian Pines in spatial resolution, spectral dimensionality, and class

Table 2. Per-class classification accuracy comparison on Indian Pines.

Class	SVM	PCA+SVM	Non-adapt.	Adapt.
Alfalfa	**.2619**	.2381	.1667	.1190
Corn-notill	**.7271**	.6703	.3538	.3491
Corn-mintill	**.5301**	.5020	.4150	.4297
Corn	**.5280**	.4813	.1028	.1028
Grass-pasture	**.8253**	.7770	.6276	.6782
Grass-trees	.9726	.9680	.9574	**.9863**
Hay-windrowed	.9791	.9814	.9768	**.9907**
Soybean-notill	.6880	.6503	.9223	**.9794**
Soybean-mintill	**.8647**	.8484	.6493	.6950
Wheat	.9946	**1.000**	.9946	.9946
Woods	**.9754**	.9754	.9508	.9684
Bldg-Grass-Tree	.4569	.3448	.4655	**.5057**
Stone-Steel-T.	.8690	.8690	.8690	**.9524**
AA	**.6646**	.6199	.5658	.5846

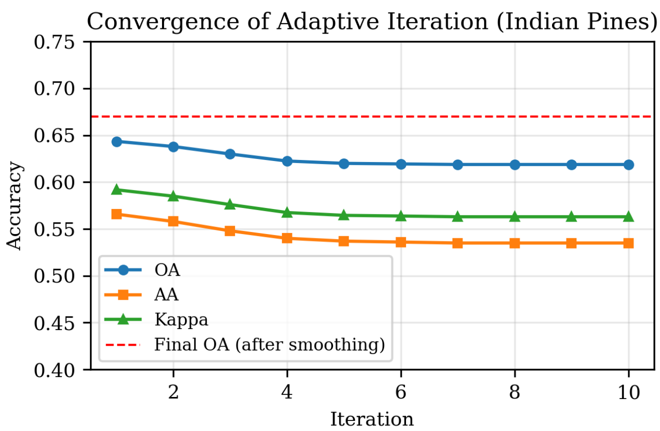

Figure 5. Convergence curve of classification accuracy during adaptive iteration on Indian Pines.

composition.

4.3.1 *Classification Accuracy Comparison*

Table 3 presents the classification accuracy comparison on Pavia University. SVM achieves the highest OA of 91.79%, while the proposed adaptive method attains an OA of 72.96% using only 15-dimensional measurements—14.6% of the original 103 spectral dimensions—achieving a 6.9-fold data compression. The relative accuracy gap between the proposed method and SVM is smaller on Pavia University than on Indian Pines in terms of the non-adaptive baseline (72.90% vs. 64.35%), which can be attributed to the lower spectral dimensionality (103 vs. 178) and the more distinct spectral signatures of urban land-cover classes.

Table 4 presents the per-class accuracy comparison.

Table 3. Classification accuracy comparison on Pavia University.

Method	OA	AA	Kappa
SVM	**0.9179**	**0.8821**	**0.8897**
PCA+SVM	0.9175	0.8817	0.8891
Fisher+SVM	0.8850	0.8445	0.8441
Non-adaptive mod.	0.7290	0.7244	0.6348
Adaptive mod.	0.7296	0.7221	0.6350

The proposed method achieves notably higher accuracy than SVM on Bitumen (99.08% vs. 74.69%) and Self-Blocking Bricks (98.43% vs. 89.86%), indicating that the Fisher discriminant encoding effectively captures the discriminative features of these classes. Conversely, for Gravel and Bare Soil, the proposed method shows lower accuracy, suggesting that the spectral signatures of these classes are less separable in the low-dimensional measurement space.

4.3.2 *Cross-Dataset Comparison and Generalizability Analysis*

Table 5 summarizes the performance of all methods across both datasets. The proposed method consistently achieves competitive classification accuracy using only 15-dimensional measurements on both datasets, confirming its generalizability. The compression ratios are 11.9× (Indian Pines) and 6.9× (Pavia University), respectively. The adaptive modulation provides a modest improvement over the non-adaptive baseline on both datasets (2.62 and 0.06 percentage points in OA after spatial smoothing, respectively). The smaller improvement on Pavia University is attributed to the already high initial

Table 4. Per-class classification accuracy comparison on Pavia University.

Class	SVM	PCA+SVM	Non-adapt.	Adapt.
Asphalt	**.9300**	.9288	.4028	.4184
Meadows	**.9876**	.9875	.9352	.9370
Gravel	**.7074**	.7011	.2328	.1831
Trees	**.9271**	.9268	.8513	.8503
Painted Metal	.9934	.9934	.9959	**.9975**
Bare Soil	**.7502**	.7488	.1646	.1495
Bitumen	.7469	.7510	.9791	**.9908**
Self-Blocking Bricks	.8986	.8998	.9695	**.9843**
Shadows	**.9977**	.9977	.9883	.9883
AA	**.8821**	.8817	.7244	.7221

classification accuracy of the non-adaptive method on this dataset.

4.4 Comparison with Probabilistic Classification Methods

To further contextualize the proposed Bayesian classification framework, a comparison with other probabilistic classification methods was conducted on both datasets. Table 6 presents the results. The methods compared include: (1) Gaussian Naive Bayes (GNB), which assumes feature independence; (2) Gaussian Mixture Model (GMM) with expectation-maximization; and (3) the proposed Bayesian classifier with Fisher encoding. All probabilistic methods operate in the same 15-dimensional measurement space.

The proposed Bayesian classifier outperforms both GNB and GMM on the Indian Pines dataset in terms of OA, AA, and Kappa. On Pavia University, GNB achieves higher OA (77.61%), AA (76.11%), and Kappa (0.7009) than the proposed method (72.90%, 72.44%, and 0.6348, respectively). GNB's superior performance on Pavia University is primarily driven by the dominant Meadows class (18,649 samples, 48.4% of all labeled pixels), whose feature independence assumption coincidentally aligns with the relatively distinct spectral signatures of urban land-cover classes. However, on Indian Pines, which contains 16 classes with more overlapping spectral features, the proposed method's use of full covariance matrices yields a substantial advantage over GNB (OA: 64.35% vs. 55.47%). The advantage over GMM on both datasets is attributed to the Fisher discriminant encoding, which maximizes inter-class separability in the measurement space, whereas GMM relies on unsupervised clustering that may not align with the true class boundaries. These results confirm that the combination of Fisher discriminant encoding and Bayesian classification provides an effective probabilistic framework for direct classification from compressed measurements, particularly on datasets with many classes and complex spectral overlap.

4.5 Data Compression Efficiency Analysis

Figure 6 compares the data dimensionality and compression ratio of each method. The proposed method requires only 15-dimensional measurements, achieving an 11.9-fold compression relative to the original 178 spectral dimensions on Indian Pines and a 6.9-fold compression relative to 103 bands on Pavia University, substantially exceeding the 5.9-fold compression of PCA+SVM on Indian Pines. Performing data compression directly at the optical front end offers three advantages: (1) the data volume acquired by the detector is significantly reduced, enabling higher acquisition speed and frame rate; (2) data transmission and storage overhead are considerably lowered, which is particularly beneficial for bandwidth-constrained platforms such as UAVs and satellites; (3) classification is performed in a low-dimensional space, reducing computational complexity from $O(P)$ to $O(K)$, which facilitates embedded real-time processing. It is worth noting that the Fisher+SVM method also uses 15-dimensional Fisher encoding, yet its classification accuracy substantially exceeds that of the Bayesian classifier in the proposed method, suggesting that the nonlinear decision boundary of SVM in the measurement space outperforms the Gaussian assumption of the Bayesian classifier. Incorporating nonlinear classifiers in future work is expected to substantially improve the classification performance of the proposed method.

Table 5. Cross-dataset performance comparison.

Method	Indian Pines OA	Indian Pines AA	Indian Pines Kappa	Pavia University OA	Pavia University AA	Pavia University Kappa
SVM	**.7828**	**.6646**	**.7497**	**.9179**	**.8821**	**.8897**
PCA+SVM	.7539	.6199	.7158	.9175	.8817	.8891
Fisher+SVM	.7511	.6109	.7121	.8850	.8445	.8441
Non-adapt.	.6435	.5658	.5918	.7290	.7244	.6348
Adapt.	.6697	.5846	.6216	.7296	.7221	.6350

Table 6. Comparison with probabilistic classification methods.

Method	Indian Pines OA	Indian Pines AA	Indian Pines Kappa	Pavia University OA	Pavia University AA	Pavia University Kappa
GNB	.5547	.4808	.4934	**.7761**	**.7611**	**.7009**
GMM	.4977	.2670	.4021	.6739	.5402	.5529
Proposed Bayesian	**.6435**	**.5658**	**.5918**	.7290	.7244	.6348

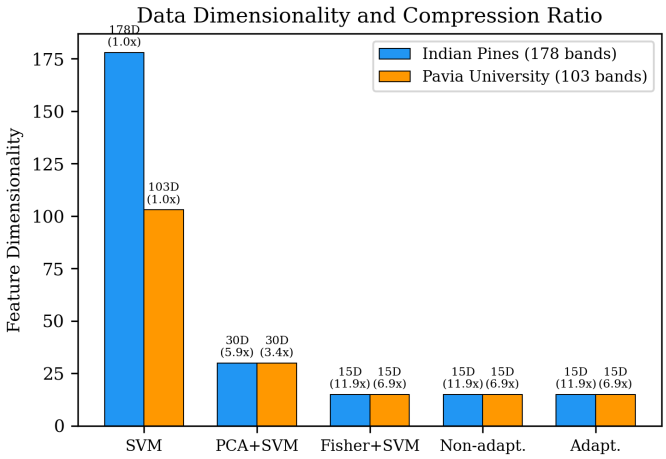

Figure 6. Comparison of data dimensionality and compression ratio among methods.

4.6 Discussion

The overall accuracy of the proposed method is lower than that of SVM, which can be attributed to three factors: (1) Information loss: compressing from 178 (or 103) to 15 dimensions inevitably sacrifices some discriminative information, particularly for classes with highly similar spectral features (e.g., Corn-notill and Corn-mintill in Indian Pines, or Gravel and Bare Soil in Pavia University), where the low-dimensional encoding fails to preserve inter-class differences; (2) Classifier limitations: the Bayesian classifier assumes Gaussian class-conditional probabilities, an assumption that may not hold in the measurement space, especially when training samples are insufficient for accurate covariance estimation; (3) Insufficient adaptive strategy: the current prior probability update does not yield significant accuracy gains during iteration, and accuracy even declines, indicating that updating priors alone is inadequate to compensate for the deficiencies of the encoding template.

Nevertheless, the significance of the proposed method lies not in achieving state-of-the-art accuracy, but in establishing a proof of concept for the "classify without reconstruction" paradigm. The improvement over the non-adaptive baseline (2.62 percentage points on Indian Pines), while modest, demonstrates that adaptive encoding template optimization can enhance classification performance without additional data acquisition. The more substantial finding is that several individual classes achieve higher accuracy than SVM (e.g., Soybean-notill: 97.94% vs. 68.80%; Bitumen: 99.08% vs. 74.69%), which indicates that the Fisher discriminant encoding captures class-specific discriminative information that is not fully exploited by SVM in the original spectral space. The 11.31% accuracy gap between the proposed method and SVM on Indian Pines represents the trade-off for an 11.9-fold reduction in data acquisition volume, which is particularly relevant for real-time applications where data throughput is a primary constraint.

Future work will focus on: (1) incorporating deep learning classifiers to replace the Bayesian classifier, enhancing nonlinear classification capability in the measurement space; (2) designing more effective adaptive encoding template optimization strategies for end-to-end joint optimization of the encoding template and classifier; (3) exploring deep learning-based encoding template design for automatic learning of classification-oriented optimal encodings; (4) validating the method on additional datasets such as Salinas; (5) constructing a physical DMD spectral imaging system to verify the method in real-world scenarios.

5 Conclusion

An adaptive hyperspectral direct classification method based on computational spectral imaging has been proposed. Classification decisions are performed directly in the measurement space through DMD encoding and modulation, circumventing the computational overhead of the conventional "reconstruct-then-classify" paradigm. The encoding template design based on Fisher discriminant analysis orients the encoding process toward classification, while the adaptive mechanism driven by posterior probability weighting provides a theoretical framework for iterative optimization of the encoding template. To address spectral aliasing caused by 2D spatial dispersion, an X-matrix extension method has been proposed for encoding template design in the 2D spatial domain. Experiments on two benchmark datasets—Indian Pines and Pavia University—confirm the feasibility and generalizability of the proposed method: overall accuracies of 66.97% and 72.96% are achieved using only 15-dimensional measurements (8.4% and 14.6% of the original spectral dimensions, respectively), with several class accuracies surpassing those of the conventional SVM method. Spatial smoothing post-processing further improves accuracy by 2.62 percentage points on Indian Pines. The proposed "classify without reconstruction" paradigm offers a new perspective for real-time hyperspectral classification and lightweight spectral imaging system design. Future efforts will focus on enhancing classification performance through deep learning classifiers and end-to-end optimization strategies.

Data Availability Statement

Data will be made available on request.

Funding

This work was supported without any funding.

Conflicts of Interest

The authors declare no conflicts of interest.

AI Use Statement

The authors declare that no generative AI was used in the preparation of this manuscript.

Ethical Approval and Consent to Participate

Not applicable.

References

[1] Bioucas-Dias, J. M., Plaza, A., Dobigeon, N., Parente, M., Du, Q., Gader, P., & Chanussot, J. (2012). Hyperspectral unmixing overview: Geometrical, statistical, and sparse regression-based approaches. *IEEE journal of selected topics in applied earth observations and remote sensing*, *5*(2), 354-379. [CrossRef]

[2] Melgani, F., & Bruzzone, L. (2004). Classification of hyperspectral remote sensing images with support vector machines. *IEEE Transactions on geoscience and remote sensing*, *42*(8), 1778-1790. [CrossRef]

[3] Yuan, X., Brady, D. J., & Katsaggelos, A. K. (2021). Snapshot compressive imaging: Theory, algorithms, and applications. *IEEE Signal Processing Magazine*, *38*(2), 65-88. [CrossRef]

[4] Hagen, N., & Kudenov, M. W. (2013). Review of snapshot spectral imaging technologies. *Optical Engineering*, *52*(9), 090901-090901. [CrossRef]

[5] Arce, G. R., Brady, D. J., Carin, L., Arguello, H., & Kittle, D. S. (2013). Compressive coded aperture spectral imaging: An introduction. *IEEE Signal Processing Magazine*, *31*(1), 105-115. [CrossRef]

[6] Candès, E. J., & Wakin, M. B. (2008). An introduction to compressive sampling. *IEEE signal processing magazine*, *25*(2), 21-30. [CrossRef]

[7] Wagadarikar, A., John, R., Willett, R., & Brady, D. (2008). Single disperser design for coded aperture snapshot spectral imaging. *Applied optics*, *47*(10), B44-B51. [CrossRef]

[8] Zhang, X., Chen, B., Zou, W., Liu, S., Zhang, Y., Xiong, R., & Zhang, J. (2024). Progressive content-aware coded hyperspectral snapshot compressive imaging. *IEEE Transactions on Circuits and Systems for Video Technology*, *34*(11), 10817-10830. [CrossRef]

[9] Wu, Z., Lu, R., Fu, Y., & Yuan, X. (2024, September). Latent diffusion prior enhanced deep unfolding for snapshot spectral compressive imaging. In *European Conference on Computer Vision* (pp. 164-181). Cham: Springer Nature Switzerland. [CrossRef]

[10] Si, Y., Lin, Z., Wang, X., & He, S. (2025). A new hyperspectral reconstruction method with conditional diffusion model for snapshot spectral compressive imaging. *IEEE Transactions on Instrumentation and Measurement*, *74*, 1–14. [CrossRef]

[11] Cao, X., Yue, T., Lin, X., Lin, S., Yuan, X., Dai, Q., ... & Brady, D. J. (2016). Computational snapshot multispectral cameras: Toward dynamic capture of the spectral world. *IEEE Signal Processing Magazine*, *33*(5), 95-108. [CrossRef]

[12] Kaarna, A., Toivanen, P., & Keränen, P. (2006). Compression and classification methods for

hyperspectral images. *Pattern Recognition and Image Analysis*, *16*(3), 413-424. [CrossRef]

[13] Zhang, H., Ma, X., Zhao, X., & Arce, G. R. (2021). Compressive hyperspectral image classification using a 3D coded convolutional neural network. *Optics Express*, *29*(21), 32875-32891. [CrossRef]

[14] Bacca, J., Galvis, L., & Arguello, H. (2020). Coupled deep learning coded aperture design for compressive image classification. *Optics express*, *28*(6), 8528-8540. [CrossRef]

[15] Yang, Q., Wang, X., Wang, D., Yu, B., Zhou, Y., & Qiao, S. (2024). Compressive hyperspectral target detection with restricted distribution property. *IEEE Transactions on Geoscience and Remote Sensing*, *62*, 1-15. [CrossRef]

[16] Yang, Q., Wang, X., Chen, L., Zhou, Y., & Qiao, S. (2024). CS-TTD: Triplet transformer for compressive hyperspectral target detection. *IEEE Transactions on Geoscience and Remote Sensing*, *62*, 1-15. [CrossRef]

[17] Chen, Y., Jiang, H., Li, C., Jia, X., & Ghamisi, P. (2016). Deep feature extraction and classification of hyperspectral images based on convolutional neural networks. *IEEE transactions on geoscience and remote sensing*, *54*(10), 6232-6251. [CrossRef]

[18] Hong, D., Han, Z., Yao, J., Gao, L., Zhang, B., Plaza, A., & Chanussot, J. (2021). SpectralFormer: Rethinking hyperspectral image classification with transformers. *IEEE Transactions on Geoscience and Remote Sensing*, *60*, 1-15. [CrossRef]

[19] Zhao, X., Ma, J., Wang, L., Zhang, Z., Ding, Y., & Xiao, X. (2025). A review of hyperspectral image classification based on graph neural networks. *Artificial Intelligence Review*, *58*(6), 172. [CrossRef]

[20] Meng, Z., Yan, Q., Zhao, F., Chen, G., Hua, W., & Liang, M. (2024). Global–Local multigranularity transformer for hyperspectral image classification. *IEEE Journal of Selected Topics in Applied Earth Observations and Remote Sensing*, *18*, 112-131. [CrossRef]

[21] Wan, X., Chen, F., Gao, W., He, Y., Liu, H., & Li, Z. (2024). Efficient spectral-spatial fusion with multiscale and adaptive attention for hyperspectral image classification. *IEEE Journal of Selected Topics in Applied Earth Observations and Remote Sensing*, *18*, 1196-1211. [CrossRef]

[22] Zhang, Z., Jiang, L., Tang, B. H., Liu, J., Wang, Q., Hu, Y., ... & Fu, Z. (2025). Attention residual hybrid network for unmanned aerial vehicles hyperspectral image classification. *IEEE Journal of Selected Topics in Applied Earth Observations and Remote Sensing*. [CrossRef]

[23] CAI, Y., TAN, M., PAN, J., & HE, K. (2024). Hyperspectral image classification based on multi-scale asymmetric dense network. *Journal of Electronics & Information Technology*, *46*(4), 1448–1457. [CrossRef]

[24] Sun, J., Zhang, H., Wang, J., Sima, H., & Jin, S. (2025). Hyperspectral Image Classification With Re-Attention Agent Transformer and Multiscale Partial Convolution. *IEEE Journal of Selected Topics in Applied Earth Observations and Remote Sensing*. [CrossRef]

[25] Correa, C. V., Arguello, H., & Arce, G. R. (2016). Spatiotemporal blue noise coded aperture design for multi-shot compressive spectral imaging. *Journal of the Optical Society of America A*, *33*(12), 2312-2322. [CrossRef]

[26] Rueda-Chacon, H., Florez-Ospina, J. F., Lau, D. L., & Arce, G. R. (2019). Snapshot compressive tof+ spectral imaging via optimized color-coded apertures. *IEEE transactions on pattern analysis and machine intelligence*, *42*(10), 2346-2360. [CrossRef]

[27] Bacca, J., Gelvez-Barrera, T., & Arguello, H. (2021). Deep Coded Aperture Design: An End-to-End Approach for Computational Imaging Tasks. *IEEE Transactions on Computational Imaging*, *7*, 1148-1160. [CrossRef]

[28] Arguello, H., Bacca, J., Kariyawasam, H., Vargas, E., Marquez, M., Hettiarachchi, R., ... & Edussooriya, C. U. (2022). Deep optical coding design in computational imaging. *arXiv preprint arXiv:2207.00164*. [arXiv]

[29] Li, W., Prasad, S., & Fowler, J. E. (2013). Hyperspectral image classification using Gaussian mixture models and Markov random fields. *IEEE Geoscience and Remote Sensing Letters*, *11*(1), 153-157. [CrossRef]

[30] He, X., Chen, Y., & Huang, L. (2023). Bayesian deep learning for hyperspectral image classification with low uncertainty. *IEEE Transactions on Geoscience and Remote Sensing*, *61*, 1-16. [CrossRef]

[31] Tarabalka, Y., Benediktsson, J. A., & Chanussot, J. (2009). Spectral–spatial classification of hyperspectral imagery based on partitional clustering techniques. *IEEE transactions on geoscience and remote sensing*, *47*(8), 2973-2987. [CrossRef]

[32] Gehm, M. E., John, R., Brady, D. J., Willett, R. M., & Schulz, T. J. (2007). Single-shot compressive spectral imaging with a dual-disperser architecture. *Optics express*, *15*(21), 14013-14027. [CrossRef]

[33] Lee, J., Son, D., Kim, H., Lee, S., Roh, J., & Yoon, J. (2025). Development of a digital micromirror device-based hyperspectral imaging system with dynamically adjustable measurement regions. *Scientific Reports*, *15*(1), 26587. [CrossRef]

[34] Kittle, D., Choi, K., Wagadarikar, A., & Brady, D. J. (2010). Multiframe image estimation for coded aperture snapshot spectral imagers. *Applied optics*, *49*(36), 6824-6833. [CrossRef]

[35] Dunlop-Gray, M., Poon, P. K., Golish, D., Vera, E., & Gehm, M. E. (2016). Experimental demonstration of an adaptive architecture for direct spectral imaging classification. *Optics express*, *24*(16), 18307-18321. [CrossRef]

[36] Bacca, J., Martinez, E., & Arguello, H. (2023). Computational spectral imaging: a contemporary overview. *Journal of the Optical Society of America A*,

40(4), C115-C125. [CrossRef]

[37] Sun, L., Zhao, G., Zheng, Y., & Wu, Z. (2022). Spectral–spatial feature tokenization transformer for hyperspectral image classification. *IEEE Transactions on Geoscience and Remote Sensing, 60*, 1-14. [CrossRef]

[38] Li, Y., Fu, X., Liu, J., & Ma, W. K. (2024). Hyperspectral Unmixing Under Endmember Variability: A Variational Inference Framework. *arXiv preprint arXiv:2407.14899*. [CrossRef]

[39] Mejia, Y., & Arguello, H. (2018). Binary codification design for compressive imaging by uniform sensing. *IEEE Transactions on Image Processing, 27*(12), 5775-5786. [CrossRef]

[40] Fang, L., Li, S., Duan, W., Ren, J., & Benediktsson, J. A. (2015). Classification of hyperspectral images by exploiting spectral–spatial information of superpixel via multiple kernels. *IEEE transactions on geoscience and remote sensing, 53*(12), 6663-6674. [CrossRef]

[41] Hong, D., Gao, L., Yokoya, N., Yao, J., Chanussot, J., Du, Q., & Zhang, B. (2020). More diverse means better: Multimodal deep learning meets remote-sensing imagery classification. *IEEE Transactions on Geoscience and Remote Sensing, 59*(5), 4340-4354. [CrossRef]

[42] He, X., Chen, Y., & Lin, Z. (2021). Spatial-spectral transformer for hyperspectral image classification. *Remote Sensing, 13*(3), 498. [CrossRef]